International Journal of Numerical Methods for Heat & F

Nanofluid flow past an impulsively started vertical plate with variable surface temperature

Rajesh Vemula A J Chamkha Mallesh M. P.

Received 6 July 2014
Revised 8 December 2014
13 January 2015
Accepted 13 January 2015

Nanofluid flow past an impulsively started vertical plate with variable surface temperature

Rajesh Vemula
Department of Engineering Mathematics, GITAM University Hyderabad Campus, Hyderabad, India
A. Chamkha
Mechanical Engineering Department, Prince Mohammad Bin Fahd University (PMU) Al-Khobar, Kingdom of Saudi Arabia, and
M.P. Mallesh
Department of Engineering Mathematics, GITAM University Hyderabad Campus, Hyderabad, India

Abstract

Purpose – The purpose of this paper is to focus on the numerical modelling of transient natural convection flow of an incompressible viscous nanofluid past an impulsively started semi-infinite vertical plate with variable surface temperature.

Design/methodology/approach – The problem is governed by the coupled non-linear partial differential equations with appropriate boundary conditions. A robust, well-tested, Crank-Nicolson type of implicit finite-difference method, which is unconditionally stable and convergent, is used to solve the governing non-linear set of partial differential equations.

Findings – The local and average values of the skin-friction coefficient (viscous drag) and the average Nusselt number (the rate of heat transfer) decreased, while the local Nusselt number increased for all nanofluids, namely, aluminium oxide-water, copper-water, titanium oxide-water and silver-water with an increase in the temperature exponent m. Selecting aluminium oxide as the dispersing nanoparticles leads to the maximum average Nusselt number (the rate of heat transfer), while choosing silver as the dispersing nanoparticles leads to the minimum local Nusselt number compared to the other nanofluids for all values of the temperature exponent m. Also, choosing silver as the dispersing nanoparticles leads to the minimum skin-friction coefficient (viscous drag), while selecting aluminium oxide as the dispersing nanoparticles leads to the maximum skin-friction coefficient (viscous drag) for all values of the temperature exponent m.

Research limitations/implications – The Brinkman model for dynamic viscosity and Maxwell-Garnett model for thermal conductivity are employed. The governing boundary layer equations are written according to The Tiwari-Das nanofluid model. A range of nanofluids containing nanoparticles of aluminium oxide, copper, titanium oxide and silver with nanoparticle volume fraction range less than or equal to 0.04 are considered.

Practical implications – The present simulations are relevant to nanomaterials thermal flow processing in the chemical engineering and metallurgy industries. This study also provides an important benchmark for further simulations of nanofluid dynamic transport phenomena of relevance to materials processing, with alternative computational algorithms (e.g. finite element methods).

Originality/value – This paper is relatively original and illustrates the influence of variable surface temperature on transient natural convection flow of a viscous incompressible nanofluid and heat transfer from an impulsively started semi-infinite vertical plate.

Keywords Nanofluids, Free convection, Implicit finite-difference numerical method, Semi-infinite vertical plate, Transient flow, Variable surface temperature

Paper type Research paper

International Journal of Numerical Methods for Heat & Fluid Flow
Vol. 26 No. 1, 2016
pp. 328-347

0961-5539
DOI 10.1108/HFF-07-2014-0209

Nomenclature

T'_w	temperature of the plate
ρ	density
μ	dynamic viscosity
ρ_{nf}	effective density of the nanofluid
μ_{nf}	effective dynamic viscosity of the nanofluid
n	empirical shape factor for the nanoparticle
ν	kinematic viscosity
ϕ	solid volume fraction of nanoparticles
T'	temperature of the fluid
T'_∞	temperature of the fluid far away from the plate
κ	thermal conductivity
κ_{nf}	thermal conductivity of the nanofluid
β	thermal expansion coefficient
β_{nf}	thermal expansion of the nanofluid
t'	time
g	acceleration due to gravity
Gr	thermal Grashof number
T	non-dimensional temperature
t	time
U	non-dimensional velocity along x-axis,
u	velocity along x-axis
v	velocity along y-axis

Subscripts

f	base fluid
nf	nanofluids
s	solid nanoparticles

1. Introduction

The transient natural convection flows over vertical bodies has wide range of applications in engineering and technology. These kinds of problems are frequently encountered in the study of enhanced heat transfer around various kinds of electrical and electronic devices, nuclear reactors. In manufacturing process such as hot extrusion, metal forming, crystal growing heat transfer effects plays an important role. In these cases the surfaces might be non-isothermal surfaces, with transient natural convection flow over a vertical plate. Therefore one has to choose the boundary conditions accordingly. With this motivation Muthukumaraswamy and Ganesan (1999) presented finite-difference solution of the transient natural convection flow of an incompressible viscous fluid past an impulsively started semi-infinite vertical plate with variable surface temperature and mass flux. Ganesan and Rani (2000) studied the problem of transient natural connective flow over a vertical cylinder with surface temperature of the cylinder varying as x^m, a power function of distance from the leading edge. Kishore *et al.* (2010) presented numerical solution of the effects of thermal radiation and viscous dissipation on unsteady laminar free convective heat and mass transfer in a viscoelastic fluid past a vertical cone with surface temperature $T' = T'_\infty + ax^m$ varying as power function of distance from the apex of the cone ($x = 0$) in the presence of a transverse magnetic field applied normal to the surface. Ahmed *et al.* (2014) investigated the effects of Darcian drag force and radiation-conduction on unsteady two-dimensional magnetohydrodynamic flow of viscous electrically conducting and Newtonian fluid over a vertical plate adjacent to a Darcian regime with variable surface temperature in presence of thermal radiation and transversal magnetic field. In all these studies a well-tested, numerically stable Crank-Nicolson finite-difference procedure is employed for the conservation equations.

However, conventional heat transfer fluids, for example oil, water and ethylene glycol mixtures, are poor heat transfer fluids because of their poor thermal conductivity. Application of these fluids as a cooling tool enhances manufacturing and operating costs. Many attempts have been taken by many researchers to enhance the thermal conductivity of these fluids by suspending nano/micro particles in liquids (Choi, 1995; Abu-Nada *et al.*, 2012). Nanofluids are made of ultrafine nanoparticles (< 100 nm) suspended in a base fluid,

which can be water or an organic solvent (Choi, 2009). Several studies have been published on the modelling of natural convection heat transfer in nanofluids: Das and Shridhar (2009) investigated natural convection heat transfer augmentation in a partially heated and partially cooled square cavity utilising nanofluids. Chamkha *et al.* (2010) studied laminar MHD mixed convection flow of a nanofluid along a stretching permeable surface in the presence of heat generation or absorption effects. Also Chamkha *et al.* (2010) presented nonsimilar solution for natural convective boundary layer flow over a sphere embedded in a porous medium saturated with a nanofluid. Rohni *et al.* (2011) studied boundary layer flow over a moving surface in a nanofluid beneath a uniform free stream. Gorla *et al.* (2011a) studied heat transfer in the boundary layer on a stretching circular cylinder in a nanofluid. Later, Gorla *et al.* (2011b) analysed the problem of mixed convective boundary layer flow over a vertical wedge embedded in a porous medium saturated with a nanofluid. Rashad *et al.* (2011) discussed natural convection boundary layer of a non-Newtonian fluid about a permeable vertical cone embedded in a porous medium saturated with a nanofluid. Chamkha *et al.* (2011) analysed the unsteady boundary layer flow of a nanofluid over a horizontal stretching plate in the presence of melting effect. Also Chamkha *et al.* (2012) studied the problem of mixed convection boundary layer flow over an isothermal vertical wedge embedded in a porous medium saturated with a nanofluid. Chamkha and Rashad (2012) investigated natural convection from a vertical permeable cone in a nanofluid saturated porous media for uniform heat and nanoparticles volume fraction fluxes. Recently Turkyilmazoglu and Pop (2013) discussed heat and mass transfer of unsteady natural convection flow of some nanofluids past a vertical infinite flat plate with radiation effect. Loganathan *et al.* (2013) studied the effects of radiation on an unsteady natural convective flow of a nanofluid past an infinite vertical plate. Makinde (2013) studied the effects of viscous dissipation and Newtonian heating on boundary layer flow of nanofluids over a flat plate. Sheikholeslami *et al.* (2014) presented a study of natural convection heat transfer in a nanofluid filled enclosure with elliptic inner cylinder. Ahmed *et al.* (2014) studied the effect of magnetic field on Soret driving free convection in an inclined porous cavity saturated by a conducting binary mixture. Turkyilmazoglu (2014) analysed unsteady convection flow of some nanofluids past a moving vertical flat plate with heat transfer by the usual Laplace transform technique.

The objective of this paper is to study the transient natural convection flow of an incompressible viscous nanofluid and heat transfer from an impulsively started semi-infinite vertical plate with variable surface temperature numerically. The governing boundary layer equations along with the initial and boundary conditions are solved by an implicit finite-difference method of the Crank-Nicolson type, which is unconditionally stable and convergent. Numerical results for the transient velocity, temperature, skin-friction coefficient and Nusselt number are presented and discussed in tables and graphs. The present study also provides an important benchmark for further simulations of nanofluid dynamic transport phenomena of relevance to materials processing, with alternative computational algorithms (e.g. finite element methods).

2. Unsteady nanofluid dynamic mathematical model

Unsteady laminar two-dimensional boundary layer free convective flow of a viscous incompressible nanofluid past an impulsively started semi-infinite vertical plate is considered. The x-axis is taken along the plate in the vertically upward direction, and the y-axis is taken normal to the surface of the plate as shown in Figure 1. The gravitational acceleration g acts downward. Initially, both the plate and the nanofluid are stationary at the same temperature T'_{∞}. They are maintained at this

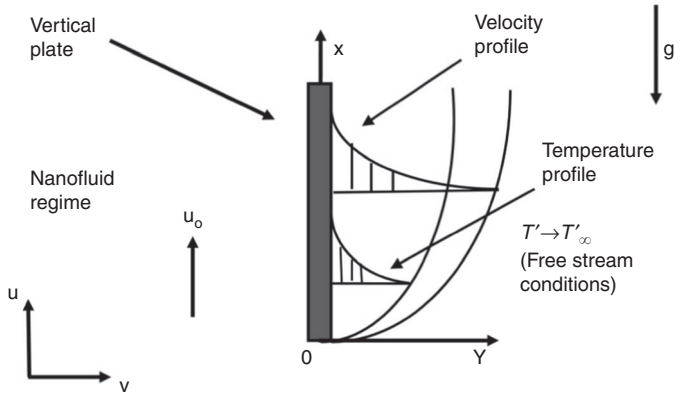

Figure 1. The physical model and coordinate system

condition for all $t' \leqslant 0$. At time $t' > 0$, the plate is given an impulsive motion in the vertically upward direction with the constant velocity u_0. The plate temperature is raised to $T' = T'_\infty + (T'_w - T'_\infty)Ax^m$, which is thereafter maintained at the same level. It is assumed that the effect of viscous dissipation is negligible in the energy equation. The fluid considered here is water-based nanofluid containing different types of nanoparticles: aluminium oxide (Al_2O_3), copper (Cu), titanium oxide (TiO_2) and silver (Ag). In this study, nanofluids are assumed to behave as single-phase fluids with local thermal equilibrium between the base fluid and the nanoparticles suspended in them so that no slip occurs between them. A schematic representation of physical model and coordinate system is depicted in Figure 1. The thermo-physical properties of the nanofluids are given in Table I (see Oztop and Abu-Nada, 2008; Loganathan *et al.*, 2013). The boundary layer and Boussinesq approximations are assumed to be valid. Under these assumptions, the governing boundary layer equations according to the model for nanofluids given by Tiwari and Das (2007) can be written in dimensional form as:

$$\frac{\partial u}{\partial x} + \frac{\partial v}{\partial y} = 0 \tag{1}$$

$$\frac{\partial u}{\partial t'} + u\frac{\partial u}{\partial x} + v\frac{\partial u}{\partial y} = \frac{\mu_{nf}}{\rho_{nf}}\frac{\partial^2 u}{\partial y^2} + \frac{(\rho\beta)_{nf}}{\rho_{nf}}g\left(T' - T'_\infty\right) \tag{2}$$

$$\frac{\partial T'}{\partial t'} + u\frac{\partial T'}{\partial x} + v\frac{\partial T'}{\partial y} = \frac{\kappa_{nf}}{\left(\rho C_p\right)_{nf}}\frac{\partial^2 T'}{\partial y^2} \tag{3}$$

	ρ(Kgm^{-3})	C_p(JKg^{-1}K^{-1})	κ(Wm^{-1}K^{-1})	$\beta \times 10^{-5}$(K^{-1})
H_2O	997.1	4,179	0.613	21
Al_2O_3	3,970	765	40	0.85
Cu	8,933	385	401	1.67
TiO_2	4,250	686.2	8.9528	0.9
Ag	10,500	235	429	1.89

Table I. Thermo-physical properties of water and nanoparticles

The initial and boundary conditions for the problem are:

$$\begin{array}{lllll} t' \leqslant 0: & u=0, & v=0, & T'=T'_{\infty} & \text{for all x and y} \\ t'>0: & u=u_0, & v=0, & T'=T'_{\infty}+\left(T'_w-T'_{\infty}\right)Ax^m & \text{at } y=0 \\ & u=0, & & T'=T'_{\infty} & \text{at } x=0 \\ & u\to 0, & & T'\to T'_{\infty} & \text{as } y\to\infty \end{array} \tag{4}$$

where $A=((u_0)/(v_f))^m$.

For nanofluids the expressions of density ρ_{nf}, thermal expansion coefficient $(\rho\beta)_{nf}$ and heat capacitance $(\rho C_p)_{nf}$ are given by:

$$\begin{aligned} \rho_{nf} &= (1-\phi)\rho_f+\phi\rho_s \\ (\rho\beta)_{nf} &= (1-\phi)(\rho\beta)_f+\phi(\rho\beta)_s \\ \left(\rho C_p\right)_{nf} &= (1-\phi)\left(\rho C_p\right)_f+\phi\left(\rho C_p\right)_s \end{aligned} \tag{5}$$

The effective thermal conductivity of the nanofluid according to Hamilton and Crosser (1962) model is given by:

$$\frac{\kappa_{eff}}{\kappa_f}=\frac{\kappa_s+(n-1)\kappa_f-(n-1)\phi\left(\kappa_f-\kappa_s\right)}{\kappa_s+(n-1)\kappa_f+\phi\left(\kappa_f-\kappa_s\right)} \tag{6}$$

where "n" is the empirical shape factor for the nanoparticle. In particular $n=3$ for spherical shaped nanoparticles and $n=3/2$ for cylindrical ones.

The following dimensionless parameters are defined:

$$\begin{aligned} &X=\frac{xu_0}{v_f}=\frac{x}{L_{ref}},\ Y=\frac{yu_0}{v_f}=\frac{y}{L_{ref}},\ t=\frac{t'u_0^2}{v_f},\ U=\frac{u}{u_0}, V=\frac{v}{u_0}, \\ &G_r=\frac{g\beta_f v_f\left(T'_w-T'_{\infty}\right)}{u_0^3},\ P_r=\frac{v_f}{\alpha_f},\ T=\frac{T'-T'_{\infty}}{T'_w-T'_{\infty}} \end{aligned} \tag{7}$$

With the non-dimensional variables (7), Equations (1)-(3) become:

$$\frac{\partial U}{\partial X}+\frac{\partial V}{\partial Y}=0 \tag{8}$$

$$\frac{\partial U}{\partial t}+U\frac{\partial U}{\partial X}+V\frac{\partial U}{\partial Y}=\frac{1}{\left(1-\phi+\phi\frac{\rho_s}{\rho_f}\right)}\left(\frac{1}{(1-\phi)^{2.5}}\frac{\partial^2 U}{\partial Y^2}+\left(1-\phi+\phi\frac{(\rho\beta)_s}{(\rho\beta)_f}\right)GrT\right) \tag{9}$$

$$\frac{\partial T}{\partial t}+U\frac{\partial T}{\partial X}+V\frac{\partial T}{\partial Y}=\frac{1}{\left(1-\phi+\phi\frac{(\rho C_p)_s}{(\rho C_p)_f}\right)}\frac{\kappa_{nf}}{\kappa_f}\frac{1}{P_r}\frac{\partial^2 T}{\partial Y^2} \tag{10}$$

The initial and boundary conditions in non-dimensional quantities are given by:

$$\begin{array}{lllll} t\leqslant 0: & U=0, & V=0, & T=0 & \text{for all X and } Y \\ t>0: & U=1, & V=0, & T=X^m & \text{at } Y=0 \\ & U=0, & & T=0 & \text{at } X=0 \\ & U\to 0, & & T\to 0 & \text{as } Y\to\infty \end{array} \tag{11}$$

$$\text{Let } E_1 = \frac{1}{(1-\phi)^{2.5}} \frac{1}{\left(1-\phi+\phi\frac{\rho_s}{\rho_f}\right)}, \quad E_2 = \frac{\left(1-\phi+\phi\frac{(\rho\beta)_s}{(\rho\beta)_f}\right)}{\left(1-\phi+\phi\frac{\rho_s}{\rho_f}\right)},$$

$$E_3 = \frac{\kappa_{nf}}{\kappa_f} \frac{1}{\left(1-\phi+\phi\frac{(\rho C_p)_s}{(\rho C_p)_f}\right)} \tag{12}$$

Now Equations (9) and (10) in terms of E_1, E_2 and E_3 are:

$$\frac{\partial U}{\partial t} + U\frac{\partial U}{\partial X} + V\frac{\partial U}{\partial Y} = E_1\frac{\partial^2 U}{\partial Y^2} + E_2 GrT \tag{13}$$

$$\frac{\partial T}{\partial t} + U\frac{\partial T}{\partial X} + V\frac{\partial T}{\partial Y} = E_3\frac{1}{P_r}\frac{\partial^2 T}{\partial Y^2} \tag{14}$$

3. Numerical technique

An implicit finite-difference scheme of Crank-Nicolson type has been used to solve the governing non-dimensional Equations (8), (13) and (14) under the initial and boundary conditions (11). The finite-difference equations corresponding to Equations (8), (13) and (14) are as follows:

$$\left[\frac{U_{i,j}^{n+1} - U_{i-1,j}^{n+1} + U_{i,j}^{n} - U_{i-1,j}^{n} + U_{i,j-1}^{n+1} - U_{i-1,j-1}^{n+1} + U_{i,j-1}^{n} - U_{i-1,j-1}^{n}}{4\Delta X}\right]$$

$$+ \left[\frac{V_{i,j}^{n+1} - V_{i,j-1}^{n+1} + V_{i,j}^{n} - V_{i,j-1}^{n}}{2\Delta Y}\right] = 0 \tag{15}$$

$$\left[\frac{U_{i,j}^{n+1} - U_{i,j}^{n}}{\Delta t}\right] + U_{i,j}^{n}\left[\frac{U_{i,j}^{n+1} - U_{i-1,j}^{n+1} + U_{i,j}^{n} - U_{i-1,j}^{n}}{2\Delta X}\right]$$

$$+ V_{i,j}^{n}\left[\frac{U_{i,j+1}^{n+1} - U_{i,j-1}^{n+1} + U_{i,j+1}^{n} - U_{i,j-1}^{n}}{4\Delta Y}\right]$$

$$= E_1\left[\frac{U_{i,j-1}^{n+1} - 2U_{i,j}^{n+1} + U_{i,j+1}^{n+1} + U_{i,j-1}^{n} - 2U_{i,j}^{n} + U_{i,j+1}^{n}}{2(\Delta Y)^2}\right]$$

$$+ \frac{G_r E_2}{2}\left[T_{i,j}^{n+1} + T_{i,j}^{n}\right] \tag{16}$$

$$\left[\frac{T_{ij}^{n+1}-T_{ij}^{n}}{\Delta t}\right]+U_{ij}^{n}\left[\frac{T_{ij}^{n+1}-T_{i-1,j}^{n+1}+T_{ij}^{n}-T_{i-1,j}^{n}}{2\Delta X}\right]$$
$$+V_{ij}^{n}\left[\frac{T_{i,j+1}^{n+1}-T_{i,j-1}^{n+1}+T_{i,j+1}^{n}-T_{i,j-1}^{n}}{4\Delta Y}\right]$$
$$=\frac{E_3}{P_r}\left[\frac{T_{i,j-1}^{n+1}-2T_{ij}^{n+1}+T_{i,j+1}^{n+1}+T_{i,j-1}^{n}-2T_{ij}^{n}+T_{i,j+1}^{n}}{2(\Delta Y)^2}\right] \quad (17)$$

The method of solving the above finite-difference equations using Thomas algorithm has been discussed by Ramachandra Prasad *et al.* (2007). The region of integration is considered as a rectangle with sides $X=0$ to $X_{\max}=1$ and $Y=0$ to $Y_{\max}=14$, where $Y_{\max}$ corresponds to $Y=\infty$ which lies very well outside the momentum and energy boundary layers. After experimenting with a few sets of mesh sizes to access grid independence, the time and spatial step sizes $\Delta t=0.01$, $\Delta X=0.05$ and $\Delta Y=0.25$ were found to give accurate results. The Crank-Nicolson implicit finite-difference scheme is always stable and convergent. The numerical computations were carried out on a Dell Laptop computer using MATLAB R2009a.

4. Exact solution and validation of numerical solution

In the absence of inertial terms, Equation (14) becomes:

$$\frac{\partial T}{\partial t}=E_3\frac{1}{P_r}\frac{\partial^2 T}{\partial Y^2} \quad (18)$$

The analytical solution of Equation (18), subject to the boundary conditions (11) (when $m=0$) by using Laplace transform method is given by:

$$T=erfc\left(\frac{y\sqrt{\Pr}}{2\sqrt{E_3 t}}\right) \quad (19)$$

To check the accuracy of the numerical results, the temperature profiles of the present study (when $m=0$) are compared with the analytical solution given by Equation (19) in Figure 2 and found to be in very good agreement. Confidence in the implicit finite-difference numerical solutions is therefore high.

5. Engineering quantities

In materials processing problems, the local skin-friction coefficient C_f, local Nusselt number Nu, average skin-friction coefficient $\overline{C_f}$ and the average Nusselt number $\overline{Nu}$ are important characteristics which are defined, respectively, as follows:

$$C_f=\frac{\tau_w}{\rho_f u_0^2}, \quad (20)$$

$$Nu=\frac{q_w L_{ref}}{\kappa_f\left(T'_w-T'_\infty\right)} \quad (21)$$

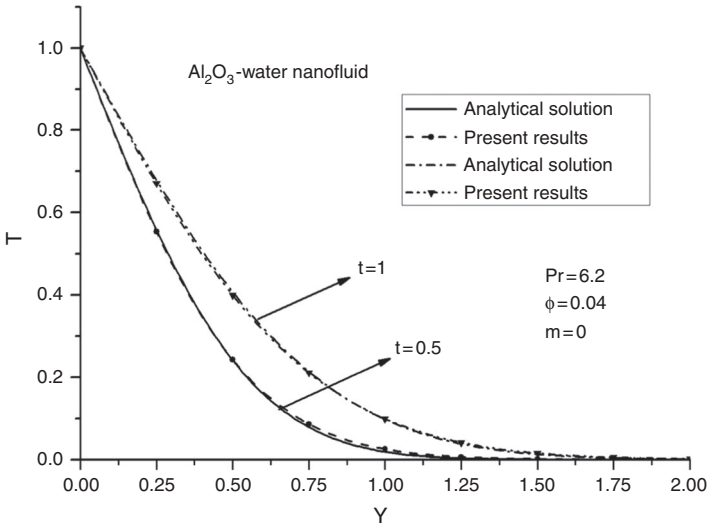

Figure 2.
Comparison of temperature profiles

$$\overline{C_f} = \frac{1}{\rho_f u_0^2 L_{ref}} \int_0^{L_{ref}} \tau_w dx \tag{22}$$

$$\overline{Nu} = \frac{1}{\kappa_f} \int_0^{L_{ref}} \frac{q_w}{(T'_w - T'_\infty)} dx \tag{23}$$

where τ_w is the skin-friction or shear stress and q_w is the heat flux or the rate of heat transfer from the surface of the plate, and they are given by:

$$\tau_w = \mu_{nf} \left(\frac{\partial u}{\partial y}\right)_{y=0}, \quad q_w = -\kappa_{nf} \left(\frac{\partial T'}{\partial y}\right)_{y=0} \tag{24}$$

Using the non-dimensional variables (7), we get the following equations.

The local skin-friction coefficient:

$$C_f = \frac{1}{(1-\phi)^{2.5}} \left(\frac{\partial U}{\partial Y}\right)_{Y=0} \tag{25}$$

The local Nusselt number:

$$Nu = -\frac{\kappa_{nf}}{\kappa_f} \left(\frac{\partial T}{\partial Y}\right)_{Y=0} \tag{26}$$

The average skin-friction coefficient:

$$\overline{C_f} = \frac{1}{(1-\phi)^{2.5}} \int_{X=0}^{1} \left(\frac{\partial U}{\partial Y}\right)_{Y=0} dX \tag{27}$$

And the average Nusselt number:

$$Nu = -\frac{\kappa_{nf}}{\kappa_f}\int_{X=0}^{1}\left(\frac{\partial T}{\partial Y}\right)_{Y=0} dX \tag{28}$$

The derivatives and integrals involved in Equations (25) to (28) are evaluated using a five-point approximation formula and Newton-Cotes closed integration formula, respectively.

6. Results and discussion

In order to get a physical insight into the problem, we have numerically evaluated the effects of significant parameters such as the thermal Grashof number (Gr), nanoparticle volume fraction (ϕ), temperature exponent (m), coordinate (X) and the time (t) on the velocity and the temperature profiles in the boundary layer region. In the present computations, the following default values for the parameters are prescribed (unless otherwise stated): $m = 0.5$, $Gr = 5$, $X = 1$, $t = 0.5$, and $\phi = 0.04$. In this study, we consider different types of nanofluids containing aluminium oxide (Al_2O_3), copper (Cu) , titanium oxide (TiO_2) and silver (Ag) nanoparticles with water as a base fluid. The nanoparticle volume fraction is considered in the range of $0 \leqslant \phi \leqslant 0.04$, as sedimentation takes place when the nanoparticle volume fraction exceeds 8 per cent. Also, we consider spherical nanoparticles with thermal conductivity and dynamic viscosity shown in Model I in Table II (see Hamilton and Crosser, 1962; Loganathan *et al.*, 2013). The Prandtl number, Pr of the base fluid is kept constant at 6.2. When $\varphi = 0$ this study reduces the governing equations to those of a regular fluid, i.e. nanoscale characteristics are eliminated.

The transient velocity and temperature profiles of Cu-water nanofluid with coordinate Y for different values of thermal Grashof number Gr are shown in Figures 3 and 4, respectively. The parameter $G_r = \left(g\beta_f v_f\left(T'_w - T'_\infty\right)\right)/\left(u_0^3\right)$ denotes the relative influence of thermal buoyancy force and viscous force in the boundary layer regime. With large values of this parameter, buoyancy effects dominate and for small values the viscous effects dominate. It is found in Figure 3 that an increase in the thermal Grashof number leads to increase in the velocity of Cu-water nanofluid. This means that the buoyancy force accelerates the velocity field. This is because an increase in the value of thermal Grashof number has the tendency to induce much flow in the boundary layer due to the effect of thermal buoyancy. But in Figure 4, the temperature of Cu-water nanofluid is found to decrease with the increase in the thermal Grashof number Gr. This means that the buoyancy force decelerates the temperature field.

Figures 5 and 6 show the effects of different values of nanoparticle volume fraction ϕ on the transient velocity and temperature profiles of Cu-water nanofluid with

Model	Shape of nanoparticles	Thermal conductivity	Dynamic viscosity
I	Spherical	$\frac{\kappa_{nf}}{\kappa_f} = \frac{\kappa_s + 2\kappa_f - 2\phi\left(\kappa_f - \kappa_s\right)}{\kappa_s + 2\kappa_f + \phi\left(\kappa_f - \kappa_s\right)}$	$\mu_{nf} = \frac{\mu_f}{(1-\phi)^{2.5}}$
II	Spherical	$\frac{\kappa_{nf}}{\kappa_f} = \frac{\kappa_s + 2\kappa_f - 2\phi\left(\kappa_f - \kappa_s\right)}{\kappa_s + 2\kappa_f + \phi\left(\kappa_f - \kappa_s\right)}$	$\mu_{nf} = \mu_f\left(1 + 7.3\,\phi + 123\,\phi^2\right)$
III	Cylindrical (nanotubes)	$\frac{\kappa_{nf}}{\kappa_f} = \frac{\kappa_s + \frac{1}{2}\kappa_f - \frac{1}{2}\phi\left(\kappa_f - \kappa_s\right)}{\kappa_s + \frac{1}{2}\kappa_f + \phi\left(\kappa_f - \kappa_s\right)}$	$\mu_{nf} = \frac{\mu_f}{(1-\phi)^{2.5}}$
IV	Cylindrical (nanotubes)	$\frac{\kappa_{nf}}{\kappa_f} = \frac{\kappa_s + \frac{1}{2}\kappa_f - \frac{1}{2}\phi\left(\kappa_f - \kappa_s\right)}{\kappa_s + \frac{1}{2}\kappa_f + \phi\left(\kappa_f - \kappa_s\right)}$	$\mu_{nf} = \mu_f\left(1 + 7.3\,\phi + 123\,\phi^2\right)$

Table II. Thermal conductivity and dynamic viscosity for various shapes of nanoparticles

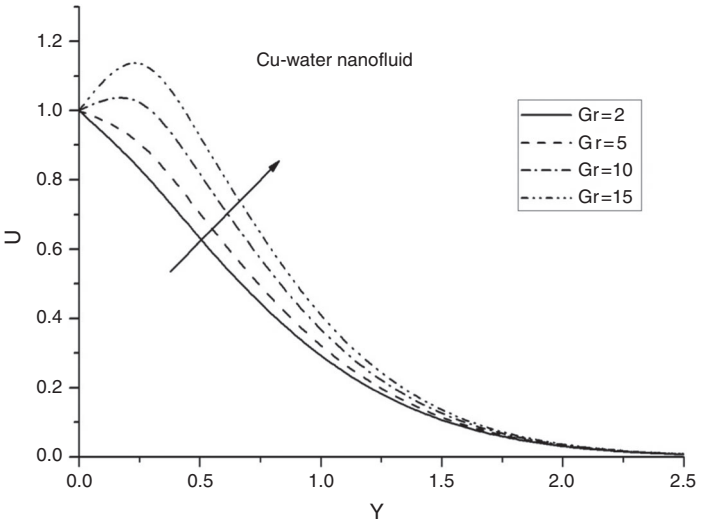

Figure 3.
Transient velocity profiles for different Gr

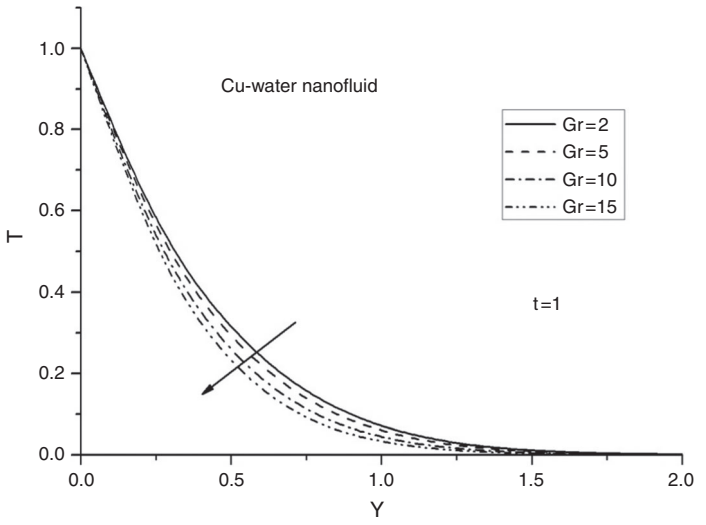

Figure 4.
Transient temperature profiles for different Gr

coordinate Y, respectively. It is found in Figure 5 that the velocity profiles of the Cu-water nanofluid decrease inside the boundary layer with the increase in the nanoparticle volume fraction ϕ. This is expected since the addition of the nanoparticles makes the fluid more viscous and thus, slows down the flow. Furthermore, it is found in Figure 6 that, the temperature profiles of the Cu-water nanofluid increase with the increase in nanoparticle volume fraction ϕ. Consequently, with increasing values of the volume fraction of the nanoparticles (Cu), the thermal boundary layer is increased. This agrees with the physical behaviour in that when the volume fraction of copper increases, the thermal conductivity increases, and then the thermal boundary layer thickness increases.

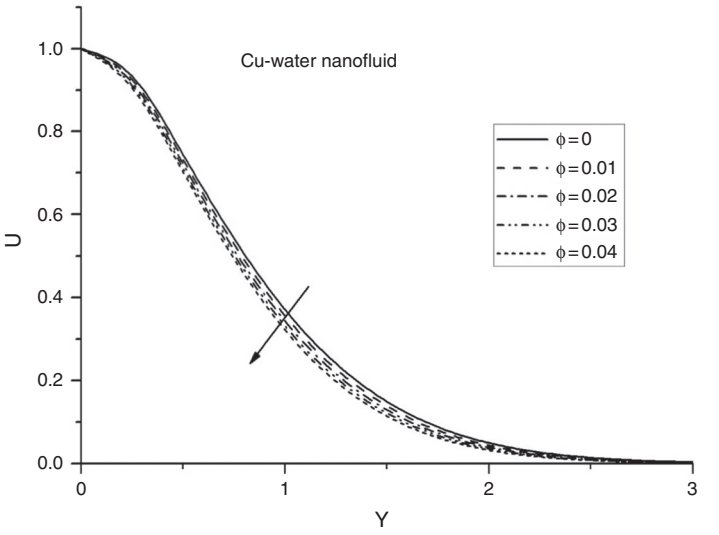

Figure 5.
Transient velocity profiles for different ϕ

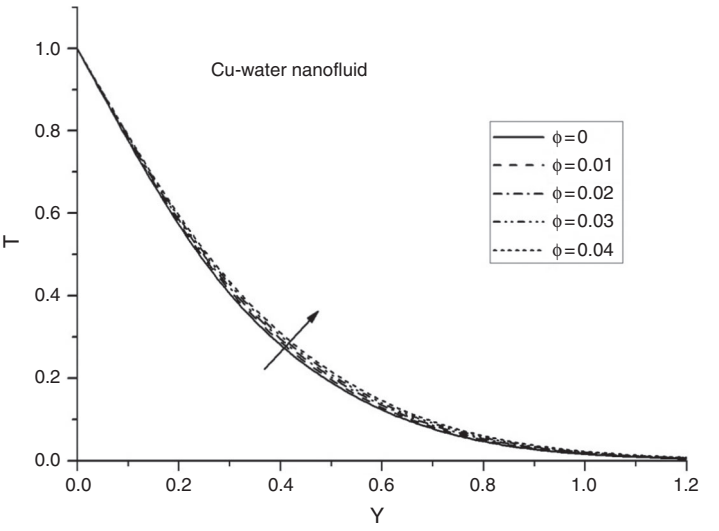

Figure 6.
Transient temperature profiles for different ϕ

The effects of different values of the temperature exponent (m) on the transient velocity and temperature profiles of Cu-water nanofluid with coordinate Y are shown in Figures 7 and 8, respectively. For m = 0, the power-law variation of the temperature at the plate surface reduces from $T' = T'_{\infty} + (T'_{w} - T'_{\infty}) Ax^{m}$ to $T' = T'_{w}$, i.e. we obtain an isothermal scenario (constant wall temperature). It is observed in Figure 7 that as m is increased, the velocity of the Cu-water nanofluid is decreased in the boundary layer while the momentum boundary layer thickness remains relatively unchanged. As such, increasing the power-law exponent in the plate surface temperature variations serves as to decelerate the flow in the boundary layer. Also, it is found in Figure 8 that the

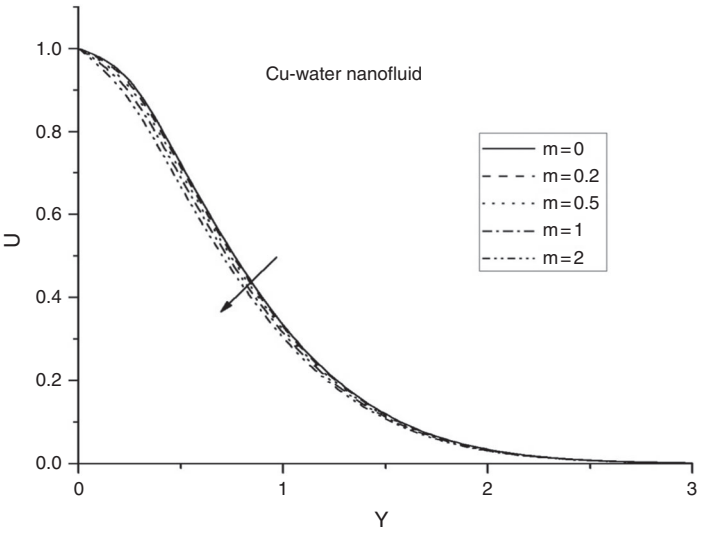

Figure 7.
Transient velocity profiles for different m

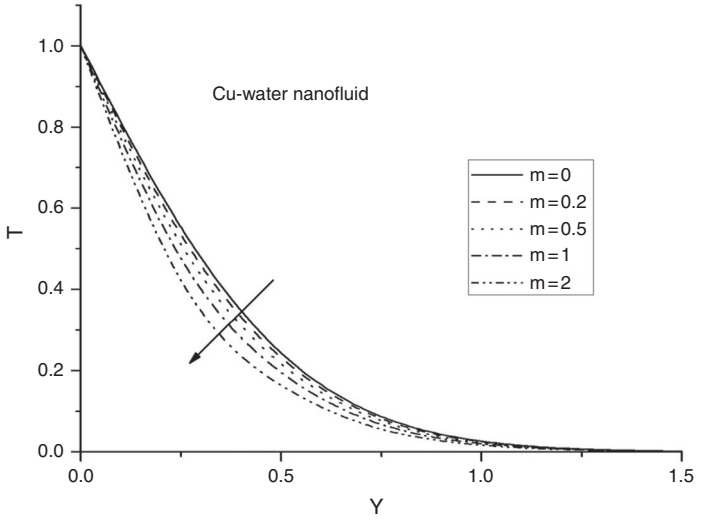

Figure 8.
Transient temperature profiles for different m

temperature profiles of the Cu-water nanofluid increase with the decrease in the exponent m with slight changes in the thermal boundary layer thickness.

Figures 9 and 10 show the development of the transient velocity and temperature profiles of Cu-water nanofluid with time t, respectively. As expected, the velocity of Cu-water nanofluid increases with a rise in time t and finally reaches the steady state. This is accompanied with significant increases in the momentum boundary layer thickness. However, as time advances, the temperature of Cu-water nanofluid is found to increase up to a certain value and then it starts decreasing and finally reaches the steady-state condition as shown in Figure 10.

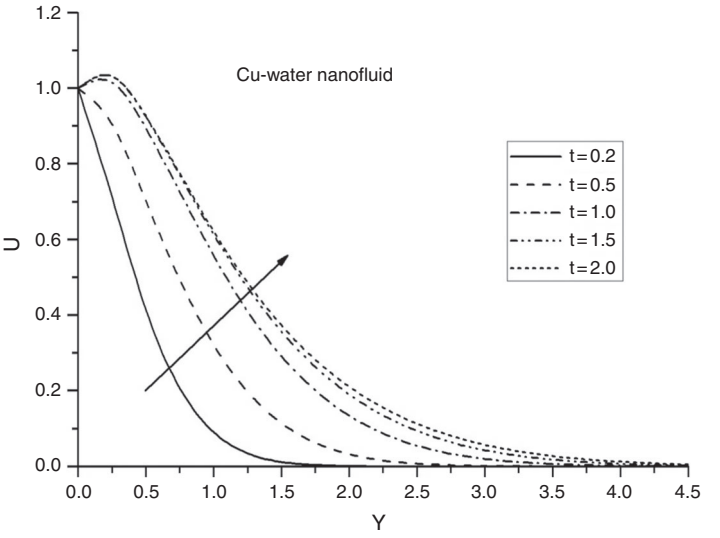

Figure 9.
Development of velocity profiles with time

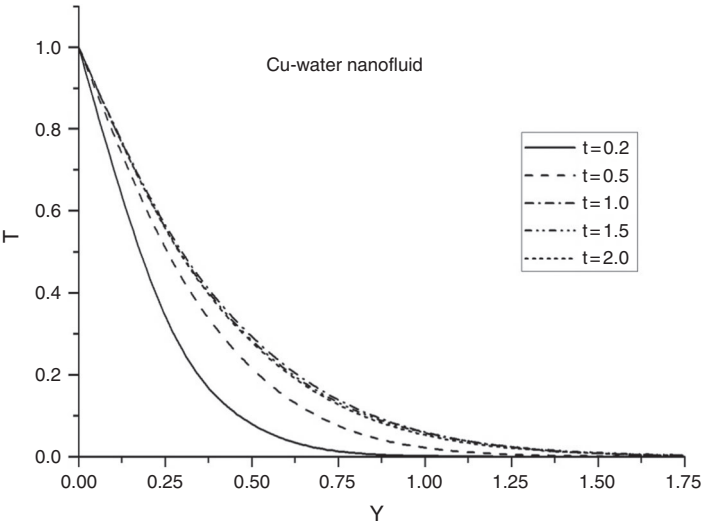

Figure 10.
Development of temperature profiles with time

Figures 11 and 12 demonstrate the influence of different values of the coordinate X on the transient velocity and temperature profiles of Cu-water nanofluid with coordinate Y, respectively. It is seen in Figures 11 and 12 that, the velocity and temperature of the Cu-water nanofluid as well as their boundary layer thicknesses increase with the increase in coordinate X. It is also observed in Figures 3-12 that the velocity and temperature of Cu-water nanofluid attains maximum at the surface of the plate or in the neighbourhood of the plate and then starts decreasing to zero monotonically with the coordinate Y for all values of Gr (thermal Grashof number), ϕ (nanoparticle volume fraction), m (exponent), t (time) and X (coordinate).

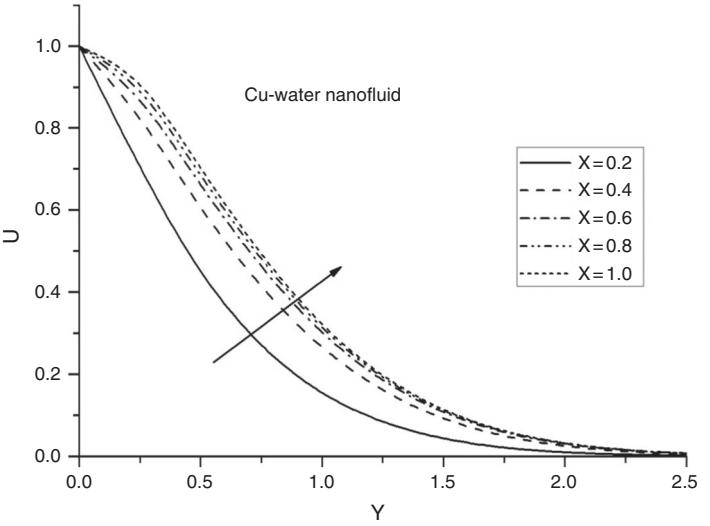

Figure 11.
Transient velocity profiles for different X

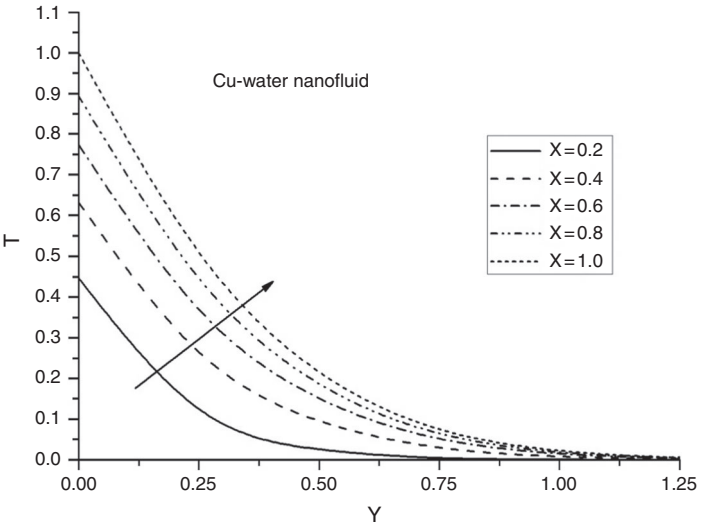

Figure 12.
Transient temperature profiles for different X

Tables III and IV demonstrate the influence of thermal Grashof number on the local and average values of the skin-friction coefficient and the Nusselt number for different types of nanofluids, namely, aluminium oxide, copper, titanium oxide and silver-water. It is observed that the local and average values of the skin-friction coefficient and the Nusselt number for all nanofluids, namely, aluminium oxide, copper, titanium oxide and silver-water increase with an increase in the thermal Grashof number. This is expected because as the thermal Grashof number increases, the strength of the convection currents increases causing increases in the wall friction and in thermal state of the nanofluid and therefore, increased heat transfer. It is also noticed that the values of the local skin-friction

coefficient, average skin-friction coefficient and the average Nusselt number are maximum corresponding to Al_2O_3-water nanofluid and minimum corresponding to Ag-water nanofluid relative to the other nanofluids for all values of the thermal Grashof number. It is also found that the local Nusselt number for TiO_2-water nanofluid is minimum for all Gr, but it is maximum for Cu-water nanofluid when $Gr = 2, 5$, also it is maximum for Al_2O_3-water nanofluid when $Gr = 10, 15$ relative to the other nanofluids. This is related to the fact to the relative thermal conductivities of these nanfluids.

Tables V and VI display the effects of the nanoparticle volume fraction ϕ on the local and average values of the skin-friction coefficient and the Nusselt number for a range of nanofluids containing nanoparticles of aluminium oxide, copper, titanium oxide and silver. From these tables, it is found that, an increase in the nanoparticle volume fraction reduces the local and average values of the skin-friction coefficient,

Table III. The local values of skin-friction coefficient and Nusselt number for different Gr

	Local skin-friction coefficient				Local Nusselt number			
Gr	Ag	Cu	TiO_2	Al_2O_3	Ag	Cu	TiO_2	Al_2O_3
2	−0.5860	−0.5654	−0.4951	−0.4879	2.6193	2.6360	2.6142	2.6349
5	0.0164	0.0335	0.1011	0.1122	2.6559	2.6726	2.6507	2.6722
10	0.9984	1.0096	1.0717	1.0890	2.7162	2.7331	2.7109	2.7336
15	1.9532	1.9584	2.0141	2.0371	2.7759	2.7929	2.7705	2.7944

Table IV. The average values of skin-friction coefficient and Nusselt number for different Gr

	Average skin-friction coefficient				Average Nusselt number			
Gr	Ag	Cu	TiO_2	Al_2O_3	Ag	Cu	TiO_2	Al_2O_3
2	−1.2717	−1.2445	−1.1553	−1.1480	2.2417	2.2594	2.2524	2.2719
5	−0.9415	−0.9167	−0.8304	−0.8207	2.2723	2.2900	2.2827	2.3028
10	−0.4084	−0.3877	−0.3069	−0.2935	2.3220	2.3398	2.3321	2.3531
15	0.1041	0.1206	0.1953	0.2120	2.3703	2.3882	2.3799	2.4019

Table V. The local values of skin-friction coefficient and Nusselt number for different ϕ

	Local skin-friction coefficient				Local Nusselt number			
ϕ	Ag	Cu	TiO_2	Al_2O_3	Ag	Cu	TiO_2	Al_2O_3
0	0.1848	0.1848	0.1848	0.1848	2.5641	2.5641	2.5641	2.5641
0.01	0.1417	0.1466	0.1646	0.1675	2.5864	2.5906	2.5855	2.5908
0.02	0.0993	0.1087	0.1439	0.1496	2.6092	2.6176	2.6071	2.6177
0.03	0.0576	0.0710	0.1228	0.1312	2.6323	2.6449	2.6288	2.6448
0.04	0.0164	0.0335	0.1011	0.1122	2.6559	2.6726	2.6507	2.6722

Table VI. The average values of skin-friction coefficient and Nusselt number for different ϕ

	Average skin-friction coefficient				Average Nusselt number			
ϕ	Ag	Cu	TiO_2	Al_2O_3	Ag	Cu	TiO_2	Al_2O_3
0	−0.6970	−0.6970	−0.6970	−0.6970	2.2023	2.2023	2.2023	2.2023
0.01	−0.7587	−0.7519	−0.7292	−0.7267	2.2190	2.2236	2.2222	2.2273
0.02	−0.8199	−0.8067	−0.7622	−0.7572	2.2363	2.2453	2.2423	2.2523
0.03	−0.8807	−0.8615	−0.7959	−0.7886	2.2540	2.2674	2.2625	2.2775
0.04	−0.9415	−0.9167	−0.8304	−0.8207	2.2723	2.2900	2.2827	2.3028

but improves the local and average values of the Nusselt number for all nanofluids, namely, aluminium oxide-water, copper-water, titanium oxide-water and silver-water. It is also seen that, Al_2O_3-water nanofluid attains maximum values of the local skin-friction coefficient, average skin-friction coefficient and the average Nusselt number, but Ag-water gets minimum values of the local skin-friction coefficient, average skin-friction coefficient and the average Nusselt number relative to the other nanofluids for all values of ϕ. On the other hand, the local skin-friction coefficient corresponding to TiO_2-water nanofluid is minimum, while it is maximum for Al_2O_3-water nanofluid and Cu-water nanofluid when $\phi = 0.01, 0.02$ and $\phi = 0.03, 0.04$, respectively. It is also observed that the local and average values of the skin-friction coefficient corresponding to pure water ($\phi = 0$) are greater than that of all considered nanofluids, while the local and average values of the Nusselt number for pure water ($\phi = 0$) are less than those of the nanofluids, namely, Al_2O_3-water, Cu-water, TiO_2-water and Ag-water nanofluids. These behaviour are related to the effect of the nanoparticle volume fraction ϕ on the corresponding calculation of the nanofluids properties as shown in Table II and therefore, their strength or weakness in conducting and transferring heat.

The effects of different values of the temperature exponent m on the local and average values of the skin-friction coefficient and the Nusselt number for various types of nanofluids, namely, aluminium oxide, copper, titanium oxide and silver are shown in Tables VII and VIII. From these tables, it is observed that the values of the local skin-friction coefficient, average skin-friction coefficient and the average Nusselt number decrease with an increase in the exponent m for all nanofluids, namely, aluminium oxide, copper, titanium oxide and silver, while the local Nusselt number increases with increasing values of the exponent m. It is also seen that the local and average values of the skin-friction coefficient are minimum corresponding to Ag-water nanofluid and maximum corresponding to Al_2O_3-water compared to the other nanofluids for all values of m. Moreover, TiO_2 achieves minimum local Nusselt number and Al_2O_3 gets maximum average Nusselt number when compared with the other nanofluids for all m.

	Local skin-friction coefficient				Local Nusselt number			
m	Ag	Cu	TiO_2	Al_2O_3	Ag	Cu	TiO_2	Al_2O_3
0	0.1238	0.1409	0.2099	0.2217	2.2021	2.2148	2.1906	2.2056
0.2	0.0779	0.0950	0.1633	0.1748	2.3943	2.4088	2.3858	2.4036
0.5	0.0164	0.0335	0.1011	0.1122	2.6559	2.6726	2.6507	2.6722
1	−0.0706	−0.0533	0.0136	0.0242	3.0345	3.0542	3.0325	3.0593
2	−0.2042	−0.1864	−0.1198	−0.1099	3.6375	3.6608	3.6368	3.6720

Table VII. The local values of skin-friction coefficient and Nusselt number for different m

	Average skin-friction coefficient				Average Nusselt number			
m	Ag	Cu	TiO_2	Al_2O_3	Ag	Cu	TiO_2	Al_2O_3
0	−0.6496	−0.6279	−0.5466	−0.5346	3.4017	3.4336	3.4376	3.4661
0.2	−0.7895	−0.7662	−0.6822	−0.6714	2.7526	2.7769	2.7755	2.7986
0.5	−0.9415	−0.9167	−0.8304	−0.8207	2.2723	2.2900	2.2827	2.3028
1	−1.1020	−1.0759	−0.9878	−0.9793	1.8101	1.8228	1.8132	1.8302
2	−1.2634	−1.2361	−1.1468	−1.1394	1.3497	1.3583	1.3496	1.3631

Table VIII. The average values of skin-friction coefficient and Nusselt number for different m

The effects of different values of time t on the local and average values of the skin-friction coefficient and the Nusselt number for different types of nanofluids, namely, aluminium oxide, copper, titanium oxide and silver are depicted in Tables IX and X. From the data in the tables, it is found that the local and average values of the skin-friction coefficient increase with a rise in time t for all nanofluids, namely, aluminium oxide, copper, titanium oxide and silver. The local and average values of the skin-friction coefficient are minimum corresponding to Ag-water nanofluid and maximum corresponding to Al_2O_3-water nanofluid relative to the other nanofluids for all t. The average Nusselt number corresponding to Al_2O_3-water nanofluid is maximum relative to the other nanofluids for all t. It is also found that the local Nusselt number is maximum for Cu-water nanofluid when t is small (t = 0.2, 0.5) and it is maximum for Al_2O_3-water nanofluid when t is large (t = 1.0, 1.5, 2.0) when compared with the other nanofluids. It is interesting to note that the local and average values of the Nusselt number decrease with a rise in t up to a certain value of t and then these values increase with time for all nanofluids, namely, aluminium oxide, copper, titanium oxide and silver. This behaviour is related to the fact seen in Figure 10 as the temperature distribution reaches a maximum before it declines to reach the steady-state values.

Table XI shows the effects of different values of the coordinate X on the local values of the skin-friction coefficient and the Nusselt number for different types of nanofluids,

Table IX.
The local values of skin-friction coefficient and Nusselt number for different t

	Local skin-friction coefficient				Local Nusselt number			
t	Ag	Cu	TiO_2	Al_2O_3	Ag	Cu	TiO_2	Al_2O_3
0.2	−1.0220	−0.9853	−0.8631	−0.8500	4.1465	4.1712	4.1294	4.1601
0.5	0.0164	0.0335	0.1011	0.1122	2.6559	2.6726	2.6507	2.6722
1.0	0.5406	0.5479	0.5864	0.5965	2.3523	2.3677	2.3526	2.3738
1.5	0.6102	0.6146	0.6445	0.6539	2.3805	2.3958	2.3794	2.4009
2.0	0.6145	0.6190	0.6488	0.6582	2.3915	2.4064	2.3886	2.4101

Table X.
The average values of skin-friction coefficient and Nusselt number for different t

	Average skin-friction coefficient				Average Nusselt number			
t	Ag	Cu	TiO_2	Al_2O_3	Ag	Cu	TiO_2	Al_2O_3
0.2	−1.5920	−1.5530	−1.4260	−1.4145	2.9602	2.9799	2.9582	2.9826
0.5	−0.9415	−0.9167	−0.8304	−0.8207	2.2723	2.2900	2.2827	2.3028
1.0	−0.7504	−0.7301	−0.6573	−0.6483	2.2206	2.2382	2.2321	2.2521
1.5	−0.7355	−0.7157	−0.6446	−0.6356	2.2318	2.2492	2.2422	2.2623
2.0	−0.7338	−0.7140	−0.6428	−0.6339	2.2342	2.2515	2.2442	2.2643

Table XI.
The local values of skin-friction coefficient and Nusselt number for different X

	Local skin-friction coefficient				Local Nusselt number			
X	Ag	Cu	TiO_2	Al_2O_3	Ag	Cu	TiO_2	Al_2O_3
0.2	−1.3166	−1.2839	−1.1776	−1.1685	2.2348	2.2558	2.2591	2.2797
0.4	−0.5835	−0.5632	−0.4922	−0.4838	2.2603	2.2788	2.2739	2.2938
0.6	−0.2845	−0.2662	−0.1990	−0.1897	2.3258	2.3424	2.3299	2.3499
0.8	−0.1160	−0.0983	−0.0307	−0.0204	2.4809	2.4971	2.4787	2.4993
1.0	0.0164	0.0335	0.1011	0.1122	2.6559	2.6726	2.6507	2.6722

namely, aluminium oxide-water, copper-water, titanium oxide-water and silver-water. From the table, the local values of the skin-friction coefficient and the Nusselt number are found to increase with increasing values of X for all nanofluids, namely, aluminium oxide-water, copper-water, titanium oxide-water and silver-water. It is also observed in Table XI that the values of the local skin-friction coefficient increases from Ag-water nanofluid to Al_2O_3-water nanofluid through Cu-water, and TiO_2-water nanofluids. This shows that the local skin-friction coefficient is minimum for Ag-water nanofluid and it is maximum for Al_2O_3-water nanofluid relative to the other nanofluids for all values of X. Moreover, it is noticed in Table XI that Al_2O_3-water nanofluid achieves the maximum value of the local Nusselt number for all $X = 0.2, 0.4, 0.6, 0.8$, while Cu attains the maximum value of the local Nusselt number at $X = 1$ relative to the other nanofluids.

7. Conclusions

In this paper, transient natural convection flow of a viscous incompressible nanofluid and heat transfer from an impulsively started semi-infinite vertical plate with variable surface temperature has been studied numerically. A range of nanofluids containing nanoparticles of aluminium oxide, copper, titanium oxide and silver is considered. A robust, well-tested, implicit finite-difference method of the Crank-Nicolson type has been used to solve the governing non-dimensional partial differential equations. The effects of significant parameters such as the thermal Grashof number, nanoparticle volume fraction, temperature exponent and the nanofluid type on the flow and heat transfer characteristics have been discussed. From the present computations, we found that as the temperature exponent m is increased, both of the velocity and temperature profiles of the Cu-water nanofluid are decreased. Also as the temperature exponent m increases, all of the local skin-friction coefficient, average skin-friction coefficient and the average Nusselt number decrease, while the local Nusselt number increases for all nanofluids, namely, aluminium oxide-water, copper-water, titanium oxide-water and silver-water. Moreover, for all values of the temperature exponent m, selecting aluminium oxide as the nanoparticle leads to the maximum average Nusselt number (the rate of heat transfer), while choosing silver as the nanoparticle leads to the minimum local Nusselt number compared to the other nanofluids. Also, choosing silver as the nanoparticle leads to the minimum skin-friction coefficient (viscous drag), while selecting aluminium oxide as the nanoparticle leads to the maximum skin-friction coefficient (viscous drag) for all values of the temperature exponent m. In addition, increasing the nanoparticle volume fraction is predicted to reduce the local and average values of the skin-friction coefficient whereas the local and average values of the Nusselt number enhance for all considered nanofluids. Moreover, the local and average values of the skin-friction coefficient and the Nusselt number increase as a result of increasing the thermal Grashof number for all considered nanofluids. The present study has examined unsteady Newtonian nanofluid transport. Future studies will investigate transient non-Newtonian nanofluid flows and will be communicated imminently.

References

Abu-Nada, E., Oztop, H.F. and Pop, I. (2012), "Buoyancy induced flow in a nanofluid filled enclosure partially exposed to forced convection", *Superlattices and Microstructures*, Vol. 51 No. 3, pp. 381-395.

Ahmed, R., Mohammed, H. and Abdelkhalk, A. (2014), "Magnetic field effect on Soret driving free convection in an inclined porous cavity saturated by a conducting binary mixture", *International Journal of Numerical Methods for Heat & Fluid Flow*, Vol. 24 No. 8, pp. 1715-1735.

Ahmed, S., Batin, A. and Chamkha, A.J. (2014), "Finite difference approach in porous media transport modelling for magnetohydrodynamic unsteady flow over a vertical plate", *International Journal of Numerical Methods for Heat & Fluid Flow*, Vol. 24 No. 5, pp. 1204-1223.

Chamkha, A.J. and Rashad, A.M. (2012), "Natural convection from a vertical permeable cone in a nanofluid saturated porous media for uniform heat and nanoparticles volume fraction fluxes", *International Journal of Numerical Methods for Heat & Fluid Flow*, Vol. 22 No. 8, pp. 1073-1085.

Chamkha, A.J., Aly, A.M. and Al-Mudhaf, H.F. (2010), "Laminar MHD mixed convection flow of a nanofluid along a stretching permeable surface in the presence of heat generation or absorption effects", *International Journal of Microscale and Nanoscale Thermal and Fluid Transport Phenomena*, Vol. 2 No. 1, pp. 51-70.

Chamkha, A.J., Gorla, R.S.R. and Ghodeswar, K. (2010), "Nonsimilar solution for natural convective boundary layer flow over a sphere embedded in a porous medium saturated with a nanofluid", *Transport in Porous Media*, Vol. 86 No. 1, pp. 13-22.

Chamkha, A.J., Rashad, A.M. and Al-Meshaiei, E. (2011), "Melting effect on unsteady hydromagnetic flow of a nanofluid past a stretching sheet", *International Journal of Chemical Reactor Engineering*, Vol. 9 No. 1, pp. 1-23.

Chamkha, A.J., Abbasbandy, S., Rashad, A.M. and Vajravelu, K. (2012), "Radiation effects on mixed convection over a wedge embedded in a porous medium filled with a nanofluid", *Transport in Porous Media*, Vol. 91 No. 1, pp. 261-279. doi: 10.1007/s11242-011-9843-5.

Choi, S. (1995), "Enhancing thermal conductivity of fluids with nanoparticles", *Developments and Applications of Non-Newtonian Flows*, FED-231/MD, Vol. 66, pp. 99-105.

Choi, S. (2009), "Nanofluids: from vision to reality through research", *Journal of Heat Transfer*, Vol. 131 No. 3, pp. 1-9.

Das, M.K. and Shridhar, O.P. (2009), "Natural convection heat transfer augmentation in a partially heated and partially cooled square cavity utilizing nanofluids", *International Journal of Numerical Methods for Heat & Fluid Flow*, Vol. 19 Nos 3/4, pp. 411-431.

Ganesan, P. and Rani, H.P. (2000), "Transient natural convection flow over vertical cylinder with variable surface temperatures", *Forschung im Ingenieurwesen*, Vol. 66, pp. 11-16.

Gorla, R.S.R., Chamkha, A.J. and Rashad, A.M. (2011a), "Mixed convective boundary layer flow over a vertical wedge embedded in a porous medium saturated with a nanofluid", *Journal of Nanoscale Research Letters*, Vol. 6 No. 207, pp. 1-9.

Gorla, R.S.R., EL-Kabeir, S.M.M. and Rashad, A.M. (2011b), "Heat transfer in the boundary layer on a stretching circular cylinder in a nanofluid", *Journal of Thermophysics and Heat Transfer*, Vol. 25 No. 1, pp. 183-186.

Hamilton, R.L. and Crosser, O.K. (1962), "Thermal conductivity of heterogeneous two component system", *Industrial & Engineering Chemistry Fundamentals*, Vol. 1 No. 3, pp. 187-191.

Kishore, P.M., Rajesh, V. and Vijayakumar Varma, S. (2010), "Viscoelastic buoyancy-driven MHD free convective heat and mass transfer past a vertical cone with thermal radiation and viscous dissipation effects", *International Journal of Applied Mathematics and Mechanics*, Vol. 6 No. 15, pp. 67-87.

Loganathan, P., Nirmal chand, P. and Ganesan, P. (2013), "Radiation effects on an unsteady natural convective flow of a nanofluid past an infinite vertical plate", *NANO: Brief Reports and Reviews*, Vol. 8 No. 1, pp. 1350001/1-1350001/10.

Makinde, D.O. (2013), "Effects of viscous dissipation and Newtonian heating on boundary-layer flow of nanofluids over a flat plate", *International Journal of Numerical Methods for Heat & Fluid Flow*, Vol. 23 No. 8, pp. 1291-1303.

Muthukumaraswamy, R. and Ganesan, P. (1999), "Flow past an impulsively started vertical plate with variable surface temperature and mass flux", *Heat and Mass Transfer*, Vol. 34 No. 6, pp. 487-493.

Oztop, H.F. and Abu-Nada, E. (2008), "Numerical study of natural convection in partially heated rectangular enclosures filled with nanofluids", *International Journal of Heat and Fluid Flow*, Vol. 29 No. 5, pp. 1326-1336.

Ramachandra Prasad, V., Bhaskar Reddy, N. and Muthucumaraswamy, R. (2007), "Radiation and mass transfer effects on two-dimensional flow past an impulsively started infinite vertical plate", *International Journal of Thermal Science*, Vol. 46 No. 12, pp. 1251-1258.

Rashad, A.M., EL-Hakiem, M.A. and Abdou, M.M.M. (2011), "Natural convection boundary layer of a non-Newtonian fluid about a permeable vertical cone embedded in a porous medium saturated with a nanofluid", *Computers & Mathematics with Applications*, Vol. 62 No. 8, pp. 3140-3151.

Rohni, M.A., Ahmad, S. and Pop, I. (2011), "Boundary layer flow over a moving surface in a nanofluid beneath a uniform free stream", *International Journal of Numerical Methods for Heat & Fluid Flow*, Vol. 21 No. 7, pp. 828-846.

Sheikholeslami, M., Ellahi, R., Hassan, M. and Soleimani, S. (2014), "A study of natural convection heat transfer in a nanofluid filled enclosure with elliptic inner cylinder", *International Journal of Numerical Methods for Heat & Fluid Flow*, Vol. 24 No. 8, pp. 1906-1927.

Tiwari, R.K. and Das, M.K. (2007), "Heat transfer augmentation in a two-sided lid-driven differentially heated square cavity utilizing nanofluids", *International Journal of Heat and Mass Transfer*, Vol. 50 Nos 9-10, pp. 2002-2018.

Turkyilmazoglu, M. (2014), "Unsteady convection flow of some nanofluids past a moving vertical flat plate with heat transfer", *ASME Journal of Heat Transfer*, Vol. 136 No. 3, pp. 031704/1-031704/7.

Turkyilmazoglu, M. and Pop, I. (2013), "Heat and mass transfer of unsteady natural convection flow of some nanofluids past a vertical infinite flat plate with radiation effect", *International Journal of Heat and Mass Transfer*, Vol. 59, pp. 167-171.

Corresponding author
Dr Rajesh Vemula can be contacted at: v.rajesh.30@gmail.com